Comparative Structural Characterization of Naturally- and Synthetically-Spun Fibers of *Bombyx mori* Fibroin

Kimberly A. Trabbic* and Paul Yager

Molecular Bioengineering Program, Department of Bioengineering, Box 352255, University of Washington, Seattle, Washington 98195

Received June 18, 1997; Revised Manuscript Received October 28, 1997

ABSTRACT: This investigation describes the comparative structural characterization of naturally- and synthetically-spun fibers of *Bombyx mori* fibroin. Wet spinning from 1,1,1,3,3,3-hexafluoro-2-propanol (HFIP) solutions was used to spin fibroin fibers with varying degrees of postspinning draw. Quantitative Raman spectroscopy showed that the secondary structure of fibroin changed dramatically from predominantly α-helical in HFIP solution to principally β-sheet in the undrawn synthetically-spun fiber. X-ray fiber diffraction showed that the undrawn fibers were highly crystalline (>50%) with little or no preferential crystalline alignment. The addition of a postspinning draw caused the polypeptide backbone and β-sheet crystals, which were formed largely by a methanol coagulation bath, to align with the fiber axis. The molecular and crystalline structures most similar to those of naturally-spun fibers were reproduced in synthetically-spun fibers with a minimum draw ratio of 2.5.

Introduction

Natural silks have become the subject of extensive study as model systems for high-performance biopolymers and polymer composites in part because of their impressive mechanical properties. For example, *Nephila clavipes* dragline silk has a specific modulus greater than that of steel and a toughness greater than that of Kevlar.[1] Although some synthetic polymer fibers also can exhibit outstanding mechanical properties, nature employs processing conditions that are chemically and physically far milder than those used in synthetic fiber processing. Biological polymers also represent a new class of potentially biodegradable materials with benign breakdown products.

Advances in molecular biotechnology and protein engineering have taken great strides toward the production of large quantities of silks and other polypeptide-based biopolymers.[2−5] However, production of useful materials, such as fibers, from this potential supply of unprocessed biopolymer requires a detailed understanding of the processing conditions necessary to induce the hierarchical structure responsible for the outstanding mechanical properties exhibited by naturally-spun fibers. While new insights into protein folding are being made for water soluble proteins, these insights have not yet had a great impact on the study of protein-based biomaterials. The materials sciences will not be able to fully capitalize on recombinantly-produced biopolymers unless techniques are developed to fold raw biopolymer properly into desired hierarchically-ordered systems.

To study the molecular basis for the formation of high-performance biopolymer fibers, we have selected to examine the spinning of fibers from *Bombyx mori* fibroin, the structural protein of *B. mori* cocoon silk, as a model system. *B. mori* cocoon fibroin is a widely studied biopolymer fiber and is commercially available in large quantities. Its extensive study over the last two thousand years has yielded a great deal of information including its molecular conformation in solution and its fibrous crystalline structure. In the aqueous solution of the silk gland, fibroin has a random coil conformation.[6−9] However, once this fibroin is spun into a cocoon fiber, the conformation of the fibroin dramatically changes to a semicrystalline structure, consisting of approximately 55% β-sheet crystallites dispersed throughout an amorphous matrix.[6,10−12] While the conformations of silk at the beginning and end of the spinning process have been determined conclusively, the mechanism for the change in conformation that accompanies spinning remains a mystery.

It has been suggested that changes in solution chemistry could cause this conformational change. Iizuka and Yang used optical rotatory dispersion and circular dichroism to investigate the effect of salts and polar organic solvents on fibroin conformation.[7,13] They found that although the fibroin remains in a random coil conformation, it becomes more contracted in the presence of salts and more expanded in the presence of urea. They also found that the addition of greater than 30% dioxane or methanol caused the fibroin to change to a β-sheet conformation. The effect of polar organic solvents on the conformation of fibroin has been confirmed also by other researchers.[14,15]

Although solvent chemistry plays a role, others have suggested that the hydrodynamic forces of fluid flow during fiber spinning might be responsible for the conformational change in fibroin. Iizuka[16,17] and Yamaura *et al.*[18,19] have presented evidence that β-sheet formation is caused by shearing forces. Iizuka suggested that there is a critical shear rate, the value of which is altered by type and quantity of cations present, for the formation of β-sheet precipitate. He proposed that the presence of multivalent cations aids in the precipitation of fibroin through the chelation of charged residues.[17] Yamaura *et al.* have presented evidence that β-sheet fibroin can be formed under shearing conditions.[18,19] Under Couette flow conditions, the amount of β-sheet precipitate formed from aqueous fibroin solutions was affected by the solution temperature, fibroin concentration, and stirrer rotation speed.

* To whom correspondence should be sent.

S0024-9297(97)00886-3 CCC: $15.00
Published on Web 01/08/1998

A few researchers have studied the *ex vivo* fiber spinning of fibroin to try to understand this dramatic conformational change. Magoshi *et al.* suggested that β-sheet fibroin is formed by elongational (*i.e.,* shear free) flow.[20] They noted that when a strands of silk were drawn from pools of *B. mori* glandular exudate at rates faster than a critical elongation rate (500 mm/min), the slopes of the stress/strain curves dramatically changed, and β-sheet precipitated in the fibers. While this study provides the strongest evidence that elongational flow is an important processing parameter for fibroin fiber spinning, these fibers were not formed from reconstituted solutions, where solution chemistries need to be defined, nor were they spun using techniques amenable to the mass production of biopolymer fibers. Yamaura *et al.* showed that fibers could be spun from reconstituted aqueous solutions of *B. mori* fibroin with specific fibroin concentrations, solution temperatures, spinning pressures, and nozzle geometries; however, their fibers lacked the β-sheet crystalline structure of naturally-spun fibers.[19] While numerous studies of *B. mori* fibroin and other silks have revealed a great deal of information concerning the crystalline states of silks as they relate to fiber spinning,[21−26] no study has conclusively identified the processing conditions needed to spin fibers with the correct hierarchical structure from reconstituted solutions of *B. mori* fibroin.

This investigation describes the first step in establishing what fibroin molecular conformation exists at all stages during the synthetic spinning of fibers from reconstituted solutions of *B. mori* fibroin. By adopting the DuPont patented process for spinning *B. mori* fibroin fibers from 1,1,1,3,3,3-hexafluoro-2-propanol (HFIP) solutions,[27] we have investigated the effect of varying degrees of postspinning draw (*i.e.,* elongational flow) on the structure of these fibers. Raman spectroscopy and X-ray fiber diffraction were used to detail the molecular and crystalline structures of fibroin. Multivariate calibration of the amide I band of Raman spectra was used to estimate the quantities of α-helix, β-sheet, β-turn, and undefined structures in synthetically and naturally spun fibroin fibers. Although fibroin is known to adopt random coil and Silk I structures under certain conditions,[6,13] these conformations were not considered during model development and, thus, cannot be predicted using this algorithm. Amide III band dichroism was used as an empirical measure of preferential polypeptide backbone alignment. These data are complementary to the crystallinity and preferential crystal orientation data obtained from x-ray fiber diffraction experiments. By comparing and contrasting the structure of the synthetically-spun fibers with that of naturally-spun fibers, we have gained a better understanding of the natural as well as the synthetic *B. mori* spinning processes. We anticipate that the information gained in this study will lead to better biomimetic spinning processes for protein-based biopolymers produced by fermentation technologies.

Materials

***B. mori* Silk Samples.** *B. mori* silk samples were obtained from raw silk yarn received from the Chul Thai Silk Co., Ltd. (Petchboon, Thailand). The yarn, like cocoons, consists of fibroin fibers that are bound together by several hydrophilic coat proteins, or sericins. Because only the hydrophobic fibroin protein was of interest to this study, the yarn was degummed to remove the sericins. Degumming was accomplished by twice boiling the silk in 20 mM Na_2CO_3 for 60 min. The degummed fibers were then washed with copious amounts of distilled water, followed by two rinses with methanol. The degummed fibroin fibers were covered in a tent of aluminum foil and allowed to air dry at 22 °C for 24 h.

***B. mori* Glandular Exudate.** Glandular silk was obtained from the posterior region of mature *B. mori* silkworms, which were raised from eggs (Carolina Biological, North Carolina) in our laboratory. The silkworms were hatched and raised in an incubator maintained at 29 °C. Because silkworms are extremely susceptible to disease, constant attention to diet, moisture, temperature, and incubator cleanliness was required for full maturation. The newly hatched worms were raised on a diet described by Suzuki and Brown.[28]

Late in the fifth instar the silkworms were dissected to retrieve glandular fibroin. Capillary samples of glandular fibroin were obtained by allowing the fibroin to drain from the posterior region of the silk gland (which only produces fibroin and not sericin) directly into a capillary tube. Raman spectra of glandular silk samples were taken immediately (within minutes) to avoid potential fibroin conformational changes due to environmental factors such as dehydration.

Methods

Spinning Silk Fibers from HFIP. *B. mori* fibroin fibers were spun synthetically using a process patented by the DuPont company.[27] Degummed *B. mori* fibroin fibers were dissolved in 9.3 M LiBr to a concentration of 17 wt % and dialyzed against distilled water for 72 h. Following dialysis the aqueous fibroin was cast into a thin film and dehydrated overnight. The solution from which fibers were spun was produced by dissolving the dehydrated fibroin film in 1,1,1,3,3,3-hexafluoro-2-propanol (HFIP) to a concentration of 15 wt % protein.

Fibers were spun using a Hamilton (South Natick, MA) syringe pump to extrude the HFIP solution through a 26 gauge hypodermic needle, through a 2 cm air gap, and into a methanol coagulation bath. The extruded filament was left in the methanol bath overnight to allow the HFIP to completely diffuse from the fiber before drawing. The filament was cut into 7 cm segments under methanol, and while still wet with methanol, the cut segments were drawn by hand to the desired draw ratio. The drawn fibers were immobilized to prevent recoil and were dried overnight at room temperature. Draw ratios of 1 (undrawn), 1.5, 2.0, 2.5, 3.0, and 3.5 were produced to examine the effect of postspinning draw on the hierarchical structure of synthetically-spun fibers. Fibers were spun and drawn in two batches. The first batch of fibers was used for X-ray fiber diffraction experiments. The second batch was used for Raman spectroscopic analysis and to estimate the error associated with the drawing process. For simplicity, fibroin fibers synthetically spun from HFIP solution will hereafter be referred to as SS-fibroin, and naturally-spun, degummed yarn fibroin will be referred to as NS-fibroin.

Hierarchical Characterization. Because fibroin fibers are semicrystalline, a thorough characterization of fibroin ordering must consider not only the molecular order but also the crystalline order. To address both levels of ordering, two complementary techniques have been adopted, Raman spectroscopy and X-ray fiber

diffraction. Laser Raman spectroscopy can reveal information about a protein's secondary structure and anisotropy. This information is complementary to the information gained from X-ray fiber diffraction, which can reveal the extent of crystallinity and preferential crystal orientation within a semicrystalline fiber. Together these techniques produce a hierarchical picture of polymer organization within fibroin fibers.

Raman Spectroscopy. Raman spectra were collected with a SPEX 500M spectrograph (Edison, NJ) equipped with a SPEX Spectrum-1, 578 × 385 pixel, liquid N_2-cooled CCD detector. Either a Lexel argon-ion laser (Fremont, CA) tuned to 514.5 nm or a Spectra Physics 3900s Ti:sapphire laser (Mountain View, CA) tuned to 740 nm was used for sample excitation. The principal axes of our 90° Raman scattering experiments were assigned according to the protocol outlined in our previous work in which the laser beam propagated along the *z*-axis, the Raman scattering was collected along the *y*-axis, and the electric vector of the laser polarization was aligned with the *x*-axis.[11,29] Spectra were collected from single fibers whose axes were oriented parallel to either the *x*-axis (axially-excited fibers) or *y*-axis (radially-excited fibers). These orientations will be referred to as the *x* and *y* orientations, respectively. All solution spectra of fibroin (*e.g.*, fibroin in 9.3 M LiBr, postdialysis fibroin solution, fibroin in HFIP, glandular exudate) were collected from capillary samples. The dehydrated fibroin film was examined on a horizontally mounted glass cover slip. Multivariate calibration of the fibroin amide I band to a basis set of protein reference spectra with known secondary structural compositions was performed to determine the fractions of α-helix, disordered helix, *β*-sheet, *β*-turn, and undefined secondary structures in fibroin samples.[30]

Spectral preprocessing prior to the multivariate calibration of the amide I band was completed according the protocol discussed previously;[11,29] however, one additional preprocessing step was performed for aqueous solutions of fibroin. Water exhibits an H−O−H bending band at approximately 1650 Δcm^{-1}, which was subtracted from the raw spectra before multivariate calibration was performed. Briefly, after background subtraction, a spectrum of distilled water was normalized to the fibroin solution spectrum by fitting the O−H stretching region (3400 Δcm^{-1}) of the water spectrum to the solution spectrum to determine the correct intensity for the water component of the spectrum. After this normalized water spectrum was subtracted from the fibroin solution spectrum, the intensity of the Raman band at 1650 Δcm^{-1} only reflected the Raman scattering due to the amide I vibrations.

The basis set of reference proteins used for multivariate calibration was created with isotropic proteins; however, fibroin fibers are anisotropic. On the basis of the assumption that the fibers are radially symmetric, a "pseudoisotropic" spectrum was created by averaging one *x*-orientation (axially excited) spectrum with two *y*-orientation (radially excited) spectra to reflect the spectrum of an isotropic fibroin sample.[11,29] The quantities of α-helix, disordered helix, *β*-sheet, *β*-turn, and undefined secondary structures predicted from the multivariate calibration of the "pseudoisotropic" spectrum, therefore, did not reflect the bias of fiber anisotropy.

Because the amide III band arises from vibrations approximately parallel to the polypeptide backbone, this band can be used to determine any preferential orientation of the backbone relative to the fiber axis. A Raman order parameter was created from the relative intensities of the amide III band of Raman spectra collected in the *x* and *y* orientations to evaluate the degree to which the polypeptide backbone was preferentially aligned with the fiber axis. This order parameter was defined as the ratio of the integrated spectral intensities between 1141 and 1433 Δcm^{-1} of spectra collected in the *x* and *y* orientations after background subtraction and normalization to the methylene deformation band at 1450 Δcm^{-1}.

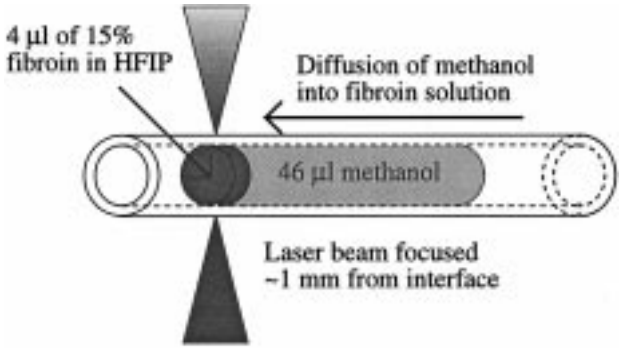

Figure 1. Schematic representation of Raman experimental geometry for investigating the precipitation of fibroin by diffusing methanol.

To determine the effect of increasing methanol concentration on the conformation of fibroin in HFIP, Raman spectra were collected from a 15 wt % solution of fibroin in HFIP as methanol was gradually introduced. Approximately 4 μL of the HFIP solution of fibroin was placed in a borosilicate glass capillary in direct contact with 46 μL of methanol. Raman spectra (740 nm Ti:sapphire excitation) were collected as a function of time at a point approximately 1 mm from the initial fibroin−methanol interface as methanol diffused into the fibroin solution. Spectra were collected from alternating spectral windows centered at 1000 and 1600 Δcm^{-1} and were used to monitor the methanol concentration and the fibroin conformation, respectively. A schematic representation of this experimental setup is shown in Figure 1. Spectral preprocessing and multivariate calibration of the amide I band were performed as previously described.[11,29]

A calibration curve for the volume percent methanol was developed using the strong spectral bands of HFIP at ∼735 Δcm^{-1} and methanol at ∼1030 Δcm^{-1}. Spectra were collected from solutions with varying HFIP and methanol concentrations. After a linear background was subtracted from each spectrum, an intensity factor, *F*, was created from the peak intensities of the HFIP, $I_{\sim 735}$, and methanol, $I_{\sim 1030}$, bands according to the following equation:

$$F = I_{\sim 735}/(I_{\sim 735} + I_{\sim 1030}) \quad (1)$$

To create a calibration curve, a third-order polynomial function was fit to the intensity factor verses methanol concentration data.

Circular Dichroism. Circular dichroism was used to confirm the secondary structure of fibroin in aqueous and HFIP solutions. Spectra were collected from a 0.1 cm path length quartz cuvette containing either a 1 μM solution of fibroin in HFIP or a 0.5 μM solution of fibroin in water using an AVIV circular dichroism spectrom-

eter, Model 62A DS (Lakewood, NJ). Four spectra were collected at a 1 nm resolution for each solution and averaged. In general, the error in the mean residue ellipticity, $[\theta]$, is less than 5% at wavelengths greater than 200 nm and less than 10% at wavelengths less than 200 nm.

X-ray Fiber Diffraction. X-ray fiber diffraction studies were carried out using a Siemens X1000 multiwire detector mounted on a Huber 4-circle goniostat. Data were collected by a personal computer running the software package, FRAMBO. X-rays were supplied from a Rigaku RU200 rotating anode with a copper target and a graphite monochromator, which was operated at 50 kV and 100 mA. X-rays were collimated with a 0.3 mm collimator. A twisted bundle of fibers was placed in a vertical orientation 8 cm from an 11 cm wide, 512 × 512 pixel detector, and patterns were collected for 15 min. These diffraction patterns were assumed to be the superposition of three X-ray scattering sources (air, amorphous fibroin, and crystalline fibroin) and an instrumental offset. Scattering from air was removed from each raw fiber diffraction pattern by subtracting an air scattering pattern, which was collected under identical instrumental conditions.

Intensity profiles were generated for the total scattering and amorphous scattering by appropriately integrating the pixel intensity of the diffraction patterns. Intensity profiles for the total scattering were obtained by radially integrating the air-subtracted diffraction patterns as a function of the Bragg angle. Intensity profiles for the amorphous scattering were calculated by radially integrating a wedge of each diffraction pattern that lacked crystallographic reflections. A wedge spanning 20° and 30° relative to the equator was integrated in all four quadrants of each diffraction pattern. The resulting intensity profile was multiplied by a factor of 9 to create an intensity profile indicative of the amorphous scattering over the entire diffraction pattern. For diffraction patterns that lacked a wedge without crystallographic reflections (*i.e.*, SS-fibroin with draw ratios less than 2.5), amorphous scattering was estimated by fitting the amorphous intensity profile of the SS-fibroin with a draw ratio of 3.5 to the amorphous intensity profiles of low draw ratio samples in regions lacking diffraction rings.

The instrumental offset, which produced a constant background pixel intensity over the entire diffraction pattern, resulted in a linearly increasing background in the integrated intensity for both the amorphous and total scattering profiles. This background was removed by subtracting a line fit to the amorphous and total intensity profiles at low Bragg angles. The resulting intensity profiles were analyzed with the software package IgorPro (WaveMetrics, Lake Oswego, OR) to estimate the crystallinity in both naturally- and synthetically-spun fibers using the following equation:

$$\% \text{ crystallinity} = [1 - (A_a/A_t)] \times 100 \qquad (2)$$

where A_a and A_t are the integrated areas of the amorphous and total scattering profiles, respectively.

The degree of preferential crystal orientation was determined from the fiber diffraction patterns. The azimuthal breadth at half the maximum intensity of the strongest equatorial reflection was used as an empirical measure of crystalline alignment.[31] Azimuthal intensity profiles were generated by integrating a 50 pixel wide ring as a function of the azimuthal angle 360° around the major equatorial reflections. Azimuthal intensity profiles were corrected for air scattering and instrumental offset using the techniques described above. Parallelism (Π), the relative measure of the azimuthal breadth at half maximum intensity of the strongest equatorial reflection, was calculated by the following equation:

$$\Pi = [1 - (H°/180°)] \times 100 \qquad (3)$$

where $H°$ is the azimuthal breadth in degrees at half maximum intensity. Using this measure, $\Pi = 0$ signifies a completely unoriented sample, and $\Pi = 100$ signifies perfectly aligned, parallel crystals.

Results and Discussion

While spinning fibroin fibers from HFIP solutions might not appear biomimetic, the physical forces involved in this spinning process qualitatively resemble those of the natural spinning process. For example, as the silkworm spins its cocoon, silk is subjected to both shearing and elongational flow conditions. Shearing forces act on the silk as it is flows through the silk gland and exits through the spinneret. During cocoon spinning the silk undergoes elongational flow after exiting the spinneret. To spin its cocoon, a silkworm secures its silk to a support and draws a strand from its body by moving its spinneret away from the point where the silk is secured. By repeatedly using this technique, the silkworm produces a cocoon fiber that has been subjected to elongational flow in short segments. In the synthetic spinning of fibroin fibers, the fibroin solution experiences shear flow during its extrusion through the hypodermic needle and elongational flow during the postspinning draw. Thus, the spinning process described in this paper produces flow conditions qualitatively similar to the flow conditions produced in silkworm cocoon spinning. However, synthetically spun fibers are considerably thicker than their naturally spun analogs. Undrawn SS-fibroin fibers are cylindrical and 163 ± 17 μm (CV (coefficient of variation) = 10.4%) in diameter. As these fibers were drawn, their diameters decreased in proportion to the inverse of the square root of the draw ratio. Also, the variability in fiber diameter was reduced with increasing draw ratio. Fibers that were subjected to a postspinning draw of 3.5 (the maximum draw before fiber breakage) have a diameter of 88 ± 6 μm (CV = 6.8%). The following molecular and crystalline characterizations of naturally and synthetically-spun fibroin fibers document the effect of elongational flow in the postspinning draw.

Molecular Characterization. The peak position of the Raman amide I band, because of its sensitivity to local protein structure, traditionally has been used to reveal the most abundant secondary structure present in proteinaceous samples. Advances in multivariate calibration now allow the information contained in the full width of this band to be used to quantitatively describe many types of protein secondary structures within a sample. Using this technique it is possible to estimate the fractions of α-helix, disordered helix, β-sheet, β-turn, and undefined structures.[30,32]

Figure 2 shows the results of the secondary structural analysis of fibroin at selected processing stages of the natural and synthetic spinning of *B. mori* fibroin. For simplicity, the α-helix and disordered helix categories have been combined into one total helix category. The changes in fibroin conformation during synthetic spin-

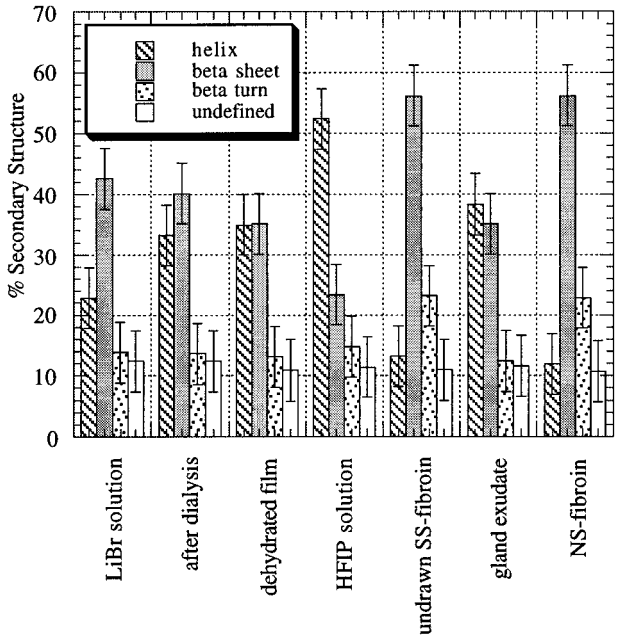

Figure 2. Secondary structural compositions of fibroin at various stages of synthetic and natural fiber spinning. Each set of data shows the percentage of helix, sheet, turn, and undefined structures ±5% error. The nearly equal concentrations of helix and sheet predicted for the glandular exudate, postdialysis solution, and dehydrated fibroin film reflect a random coil conformation for which this algorithm cannot analyze directly. Fibroin in HFIP is the only solution that clearly has a highly α-helical structure. Once this solution is synthetically spun into a fiber, a 10% increase in β-turn is observed, and the dominant secondary structure of the fibroin dramatically changes to β-sheet. The secondary structural compositions of SS-fibers and NS-fibers are very similar.

ning are as follows. A solution of 17% fibroin by weight in 9.3 M LiBr exhibits a slightly increased helical content and a slightly decreased β-sheet content compared to the fibers from which the solution was made. After dialysis against distilled water, the solution (approximately 10% fibroin by weight) contains nearly equal quantities of α-helix and β-sheet as does the thin film that was cast from this solution. Both the solution following dialysis and the dehydrated film have secondary structural compositions that greatly resemble that of glandular exudate. Fibroin in HFIP adopts a conformation that is more than 50% α-helix and only 24% β-sheet. The spinning of this solution to form an undrawn fiber dramatically changes the secondary structural composition to one very similar to that observed in naturally-spun fibers: 56% β-sheet, 13% α-helix, 23% β-turn, and 11% undefined. The 10% increase in β-turn structure in both NS- and SS-fibers is consistent with the formation of antiparallel β-sheet crystals in the fiber.

Since random coil and silk I conformations were not considered during Williams' model development for the calibration of the amide I band,[30] it was important to understand how these conformations would manifest themselves in the results of this algorithm. Fibroin obtained from the posterior region of the *B. mori* silk gland as well as the postdialysis fibroin solution have been determined to be random coil by a variety of techniques;[6−9] however, this algorithm predicts a conformation containing nearly equal quantities of α-helix and β-sheet with approximately 10% turn and undefined structures. A similar secondary structure is predicted

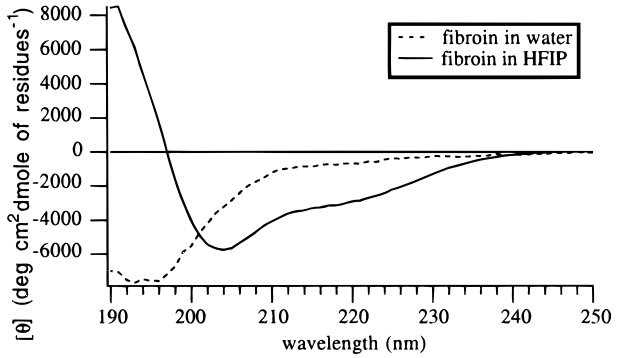

Figure 3. CD spectra of fibroin in aqueous and HFIP solutions showing that fibroin adopts different conformations in these two solvents. Aqueous fibroin exhibits a spectrum very similar to a classical random coil conformation with negative extremum in ellipticity at 195 nm. The absence of a crossover to a positive ellipticity at higher wavelengths probably indicates the presence of a small fraction of β-sheet. Fibroin in HFIP has a spectrum very similar to that of poly-L-alanine, which adopts a "doubly hydrogen-bonded" helix in HFIP.[34]

for the fibroin film, which should have a silk I structure.[6] Since this algorithm consistently predicts approximately 10% β-turn (in the absence of a highly β-sheet sample) and 10% undefined structures, nearly equal quantities of helix and sheet structures must reflect the presence of random coil or silk I conformations and not necessarily the presence of true helix and sheet structures. While it is theoretically possible for a protein to have this exact secondary structural composition resulting from the presence of true helix and sheet structures, it would be indistinguishable from a random coil conformation from the standpoint of this algorithm. Likewise, random coil and silk I structures would be indistinguishable from each other.

To further distinguish the random coil conformation of aqueous fibroin from the true helical content of fibroin in HFIP, circular dichroism (CD) was performed. Figure 3, which shows the CD spectra of fibroin dissolved in water and HFIP, confirms that the fibroin adopts quite different conformations in these two solvents. Fibroin in water adopts a largely random coil conformation as indicated by the negative extremum in ellipticity at 195 nm. This solution might contain a small fraction of β-sheet structure since the ellipticity is negative at all wavelengths investigated. A slight β-sheet content in the aqueous fibroin is consistent with the secondary structural composition determined from Raman spectra for the fibroin following dialysis. This observation is consistent with the conformations determined from CD spectra of other aqueous fibroin samples found in the literature.[7,13,33] In contrast, the spectrum of fibroin in HFIP is consistent with the structure of poly-L-alanine in HFIP as described by Parrish and Blout.[34] Their CD spectrum of poly-L-alanine in HFIP exhibits a negative shoulder at 219 nm, a larger negative extremum 204 nm, a crossover point between 198 and 197 nm, and a positive extremum at 189 nm. They postulated that the polypeptide conformation that produces this CD spectrum is a doubly hydrogen-bonded helix described as a "distorted α-helix in which the peptide carbonyl groups point slightly out from the helix axis and are hydrogen bonded simultaneously both to the NH of the fourth peptide residue to the carboxyl terminal side (as in the classical α-helix), as well as to a solvent molecule's hydroxyl hydrogen."[34] Since fibroin is 29.3% alanine and 44.5% glycine,[35] it is not unreasonable that fibroin

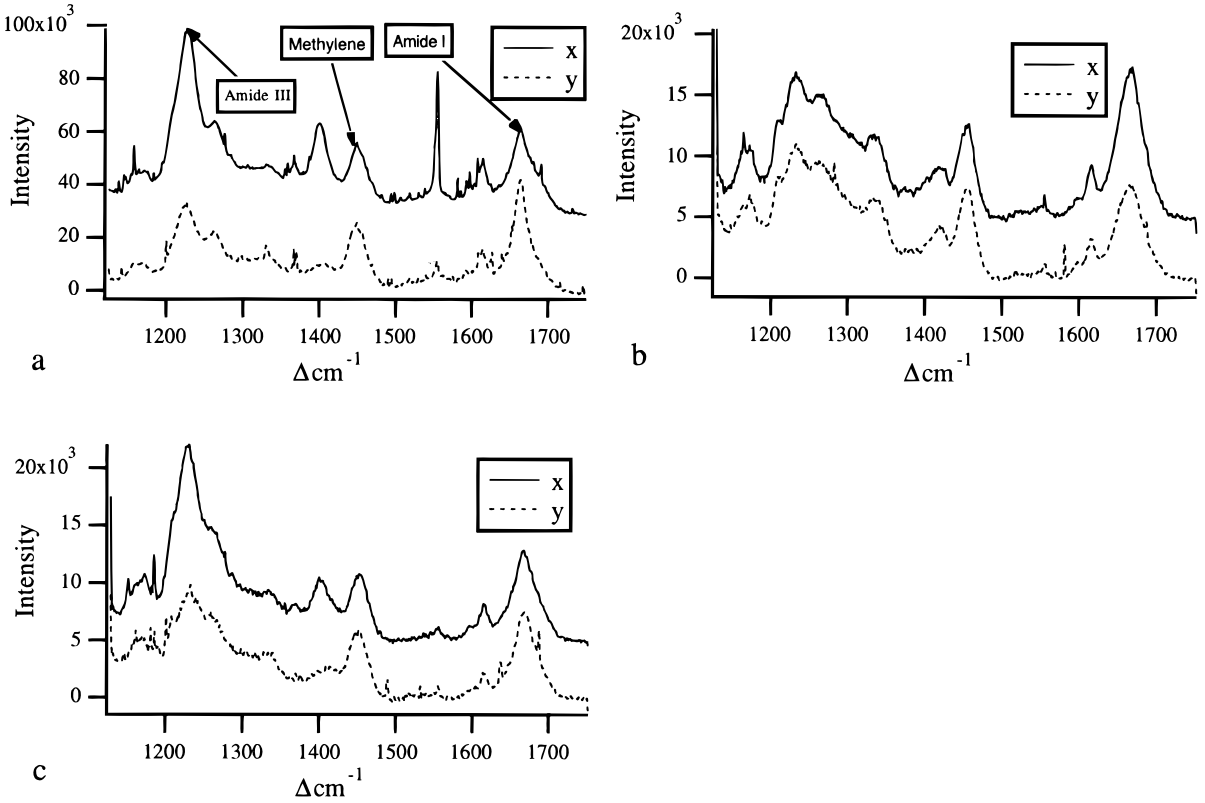

Figure 4. Raman spectra of NS- and SS-fibroin fibers collected in the *x* and *y* orientations: (a) NS-fibroin; (b) SS-fibroin with no postspinning draw; (c) SS-fibroin with postspinning draw of 3.5. The amide I band peak position at ~1670 Δcm^{-1} suggests that all the fibroin fibers are comprised largely of β-sheet; however, amide III band dichroism suggests that the polypeptide backbone has no preferential orientation in undrawn, SS-fibroin fibers, but, like NS-fibers, the backbone becomes aligned preferentially with the fiber axis in highly-drawn SS-fibers.

in HFIP would adopt a conformation similar that of to poly-L-alanine in HFIP.

Orientation of the polypeptide backbone may be determined from the dichroism of the Raman amide I and amide III bands. Since the amide III band arises primarily from the stretching of carbon−nitrogen bonds of the polypeptide backbone, increases in amide III band intensity indicate an increase in the alignment of these bonds (and the polypeptide backbone) with the laser polarization. Conversely, the amide I band arises primarily from the stretching of carbon−oxygen double bonds, which are oriented orthogonal to the polypeptide backbone. Thus, increases in amide I intensity indicate a decrease in the alignment of the polypeptide backbone with the laser polarization. By comparison of Raman spectra collected from fibrous samples oriented in axially-excited (laser polarization parallel to the fiber axis) and radially-excited (laser polarization perpendicular to the fiber axis) geometries, the orientation of the polypeptide backbone with respect to the fiber axis can be determined.

While the secondary structural compositions of the undrawn, SS-fibroin fibers and NS-fibroin fibers (Figure 2) indicate they have very similar secondary structures, examination of amide I and III band intensities reveals that the preferential orientation of the polypeptide backbone dramatically differentiates the two fibers (Figure 4a,b). The NS-fiber (Figure 4a) has a more intense amide III band in the *x* orientation and a more intense amide I band in the *y* orientation. These differences in spectral band intensities reveal that the polypeptide backbone is preferentially aligned with the fiber axis in NS-fibroin fibers. In contrast, undrawn SS-fibroin (Figure 4b) shows very little amide I and III band dichroism, suggesting little or no preferential polypeptide backbone alignment. The addition of a postspinning draw to the spinning process has a dramatic effect on the preferential polypeptide alignment of SS-fibroin fibers. Figure 4c shows spectra taken in the *x* and *y* orientations of SS-fibroin that was subjected to a postspinning draw of 3.5. These spectra show amide I and III band dichroisms qualitatively similar to those of NS-fibroin fibers.

The extent of preferential backbone alignment varies greatly with the extent of postspinning draw and can be semiquantitatively described by an order parameter created from the ratio of the amide III band intensities of spectra collected in the *x* and *y* orientations. A plot of this Raman order parameter with the degree of postspinning draw (Figure 5) shows that the undrawn, SS-fibroin has the lowest degree of molecular alignment. The order parameter increases with increasing postspinning draw ratio until the values level off at draw ratios of 2.5 and greater. Relatively little change in the Raman order parameter occurs at draw ratios greater than 2.5, where the degree of molecular alignment exhibited by the SS-fibroin is very similar to that exhibited by NS-fibroin.

Secondary structural analysis of fibrous samples can reveal information about the quantity and orientation of specific secondary structures. Table 1 summarizes the secondary structural compositions of NS-fibroin, SS-fibroin with no postspinning draw, and SS-fibroin with a postspinning draw of 3.5 for spectra collected in the *x* and *y* orientations. Table 1 also includes analysis of the "pseudoisotropic" spectrum, which reflects the secondary

Table 1. Secondary Structural Compositions of NS- and SS-Fibroin Fibers (±5%)[a]

B. mori fiber	orientation	α-helix (%)	disordered helix (%)	β-sheet (%)	β-turn (%)	undefined (%)
NS-fibroin	*x*	8.4	10.2	48.6	20.9	10.2
	y	5.5	7.0	58.1	23.6	11.1
	"pseudoisotropic"	5.6	7.0	56.5	23.1	10.9
SS-fibroin undrawn	*x*	5.7	7.1	56.4	23.2	10.9
	y	6.0	7.3	56.0	23.2	11.0
	"pseudoisotropic"	5.9	7.3	56.2	23.2	11.0
SS-fibroin 3.5 draw	*x*	6.5	8.3	53.3	21.7	10.4
	y	1.4	3.6	64.2	23.0	10.5
	"pseudoisotropic"	2.9	4.8	60.7	22.8	10.5

[a]Note: random coil and silk I structures were not considered.

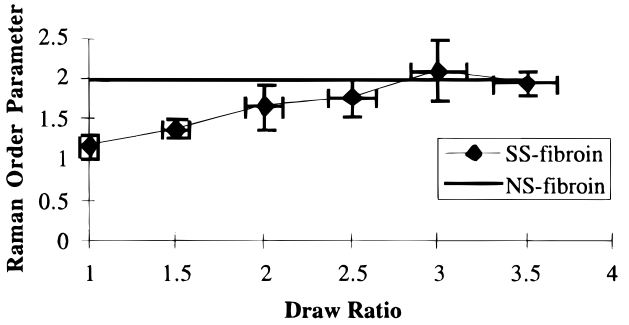

Figure 5. Effect of postspinning draw ratio on Raman order parameter. Error bars in the *y*-axis reflect the first standard deviation in the measurement of four samples, two of which were measured three times for each draw ratio. Error bars in the *x* orientation reflect the first standard deviation in the error associated with the drawing process. The Raman order parameter, which describes the preferential alignment of the polypeptide backbone with the fiber axis, in NS-fibers is approximated in SS-fibers with a postspinning draw of at least 2.5. Little increase in the Raman order parameter is produced with draw ratios greater than 2.5.

structure without the bias of fiber anisotropy. The overall secondary structural composition of SS-fibroin that is simply extruded and not subjected to a postspinning draw is very similar to that of NS-fibroin (Table I); however, the preferential alignment of the secondary structures in the undrawn SS-fibroin differs greatly from that of the NS fibroin. The alignment of amide carbonyls from specific secondary structures with the laser polarization leads to increased amide I band intensity at Raman shifts corresponding to those structures. This results in an apparent increase in the concentrations of those structures in specific collection orientations for anisotropic samples. Increased α-helix concentrations in the *x*-orientation (relative to the *y* orientation) indicates the alignment of α-helical structures parallel to the fiber axis. Likewise, increased β-sheet concentrations in the *y* orientation (relative to the *x* orientation) indicates alignment of β-sheet structures parallel with the fiber axis. NS-fibroin fibers exhibit greater β-sheet concentrations in the *y* orientation suggesting that the β-sheets are preferentially aligned parallel to the fiber axis. However, undrawn SS-fibroin exhibits nearly equal quantities of β-sheet in both the *x* and *y* orientations indicating that unlike the NS-fibroin fibers, the β-sheet of undrawn SS-fibroin is randomly oriented.

The postspinning draw changes the overall secondary structural composition of SS-fibroin fibers. A modest (~5% with a draw ratio of 3.5) increase in β-sheet and decrease in α-helical structures is caused by the postspinning draw as indicated by the pseudoisotropic composition. Also, fibers that were removed from the methanol coagulation bath within 2 h of extrusion exhibited reduced β-sheet and increased α-helix content (data not shown), which was easily converted to β-sheet with a minimum draw ratio of 1.5. Thus, the elongational flow of the post spinning draw can cause the conversion of α-helix to β-sheet.

The postspinning draw also causes the preferential alignment of α-helices and β-sheets. A slightly greater β-sheet content in the *y* orientation (relative to *x* orientation) indicates that the β-sheets of drawn SS-fibroin fibers are preferentially aligned with the fiber axis. Similarly, a slightly greater helix (both α-helix and disordered) in the *x* orientation indicates that the helices of drawn SS-fibroin fibers are also preferentially aligned with the fiber axis. This preferential alignment is exhibited by NS-fibroin fibers but not by the undrawn SS-fibroin fibers, which exhibit nearly equal secondary structural compositions in both the *x* and *y* orientations. Thus, drawing produces a secondary structural alignment similar to that observed in NS-fibroin fibers.

Crystalline Characterization. X-ray fiber diffraction was used to explore the crystalline organization of SS- and NS-fibroin fibers. Figure 6 shows the diffraction patterns collected from SS-fibroin with no postspinning draw, SS-fibroin with a postspinning draw of 2.0, SS-fibroin with a postspinning draw of 3.5, and NS-fibroin. A qualitative examination of these diffraction patterns reveals a marked similarity between the NS-fibroin and highly-drawn SS-fibroin fibers. All the major reflections are present in both the natural (Figure 6d) and highly-drawn SS-fibroin fibers (Figure 6c), suggesting that their crystalline structures are very similar. The patterns also show the effect that draw ratio has on the preferential orientation of crystallites. The diffraction pattern of the undrawn SS-fibroin has very uniform diffraction rings, showing that the crystals are randomly oriented. Increasing the draw ratio concentrates the scattering intensity at equatorial reflections, suggesting that the crystallites are becoming increasingly aligned with the fiber axis.

Quantitative analysis of the diffraction patterns yields much richer insight into the crystalline structure of SS-fibroin. Scattering intensity profiles due to the crystalline and amorphous fractions were calculated after performing image processing necessary to remove air scattering and instrumental offset from each diffraction pattern. The crystallinity was estimated according to eq 2 and plotted as a function of the draw ratio (Figure 7). The crystallinity of SS-fibroin is slightly greater than that of NS-fibroin and increases slightly with increasing postspinning draw ratio. This is in direct agreement with the secondary structural analysis of Raman spectra of these samples, which indicated a slight increase β-sheet with increasing draw ratio.

The addition of a postspinning draw changes the extent of preferential crystalline alignment, which can

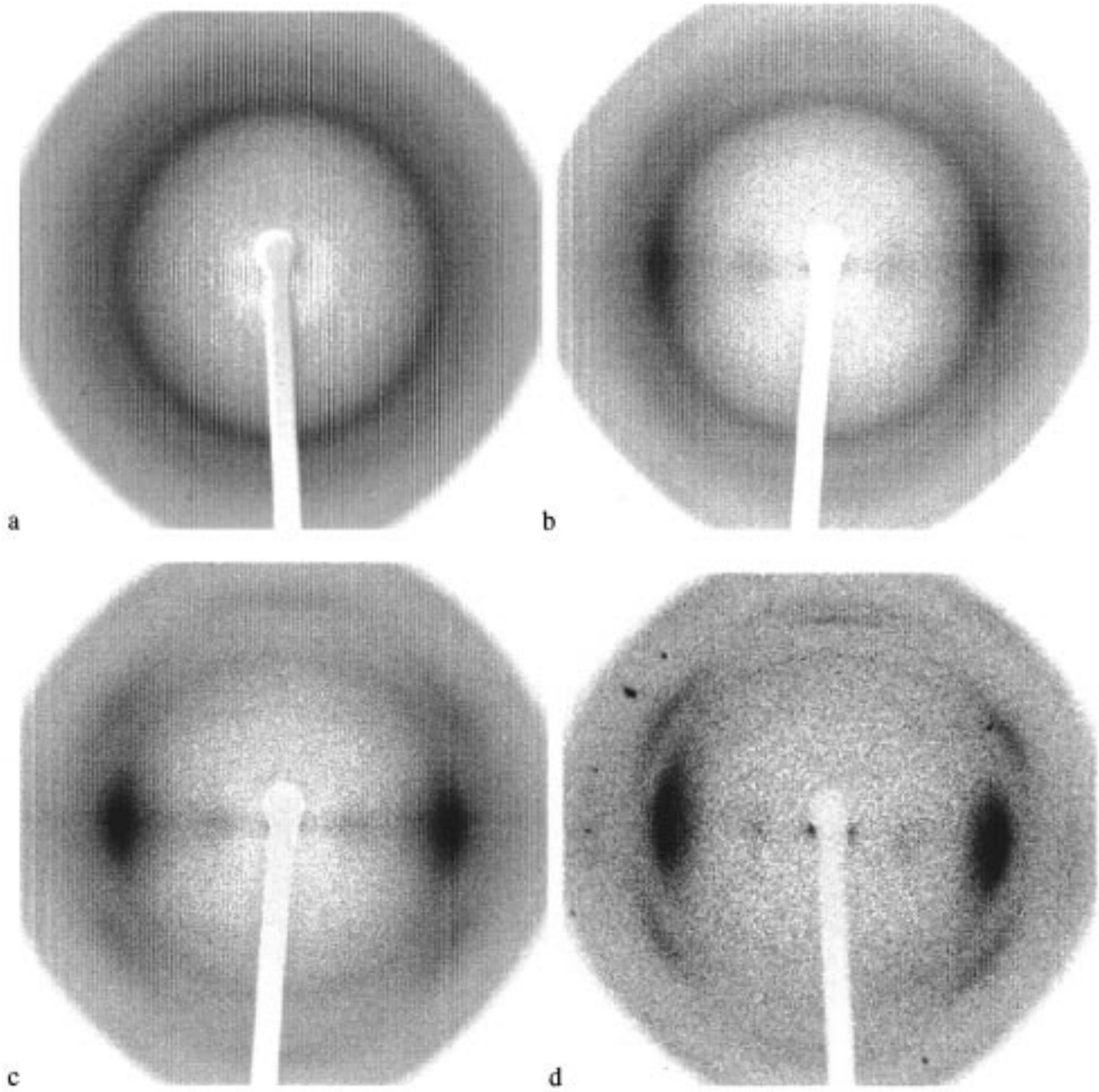

Figure 6. X-ray diffraction patterns of NS-fibroin and SS-fibroin twisted fiber bundles: **(**a) undrawn SS-fibroin; (b) SS-fibroin with a postspinning draw of 2.0; (c) SS-fibroin with a postspinning draw of 3.5; (d) NS-fibroin. The contrast of each pattern has been digitally enhanced for viewing purposes. Data analysis was performed on unenhanced diffraction patterns. Fiber bundle orientation was vertical in all diffraction patterns. Uniform diffraction rings show that undrawn SS-fibers have unoriented crystallites. Concentration of diffraction intensity at the equator shows that the crystallites become increasingly aligned with the fiber axis with increasing draw ratio. The diffraction pattern of SS-fibers with a postspinning draw ratio of 3.5 is qualitatively similar to that of NS-fibers, suggesting that their overall crystalline structure is very similar; however, the diffuse nature of the SS-fiber pattern suggests that the crystallites in SS-fibers are more disordered than those in NS-fibers.

be determined by integrating diffraction intensities with respect to the azimuthal angle of a 50 pixel wide ring encompassing the major equatorial peaks. The full width at half-maximum intensity of a major equatorial peak can be used as a practical measure of crystalline alignment.[31] The relative measure of this peak breadth, parallelism (see equation 3), is plotted against the degree of postspinning draw in Figure 8. The degree of parallelism seen in NS-fibroin is achieved in SS-fibroin with a postspinning draw ratio equal to or greater than 2.5. No further crystalline alignment appears to be accomplished with draw ratios greater than 2.5.

Role of Coagulation Bath Chemistry. It is clear from the spectroscopic and crystallographic data presented in the preceding sections that large conformational changes accompany the spinning of SS-fibroin. Unlike its natural analog (aqueous glandular fibroin), fibroin in HFIP has a high degree of α-helical content, which is converted to unoriented β-sheet crystallites dispersed throughout an amorphous matrix upon extrusion through an air gap and into a methanol coagulation bath. The postspinning draw is responsible for the preferential alignment of the polypeptide backbone as well as the β-sheet crystallites parallel to the fiber axis. Drawing also seems to be responsible for the conversion

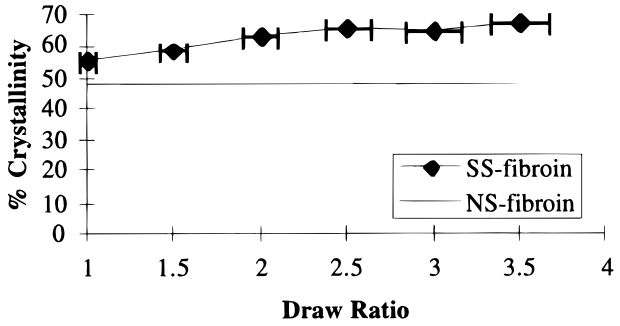

Figure 7. Effect of post-spinning draw on the crystallinity of SS-fibroin fibers. The crystallinity of all SS-fibers is slightly higher than that of NS-fibers, and the crystallinity increases very slightly with draw ratio.

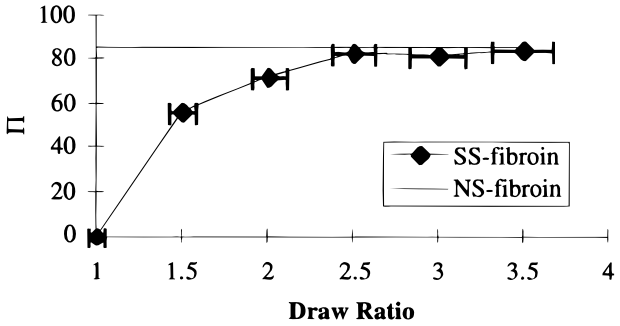

Figure 8. Effect of postspinning draw on the parallelism, Π, of crystallites in SS-fibroin fibers. Parallelism, a relative measure of the preferential crystal alignment, shows that crystallites in SS-fibers become increasingly aligned with the fiber axis with increasing draw ratio. The parallelism in NS-fibers is reproduced in SS-fibers with a postspinning draw of at least 2.5. No further increase in the parallelism is produced with draw ratios greater than 2.5.

of a small amount of α-helix in the extruded fibers to β-sheet resulting in a slightly higher than normal concentration of β-sheet in the highly-drawn SS-fibroin fibers. A large conformational change from α-helix to β-sheet occurs during the spinning of SS-fibroin, but it is unclear whether the coagulation bath chemistry or the fibroin flow is responsible for this large conformational change.

To test if the methanol coagulation bath was responsible for the conformational change in fibroin during SS-fiber spinning, fibroin conformation was monitored using Raman spectroscopy in the absence of shear as a

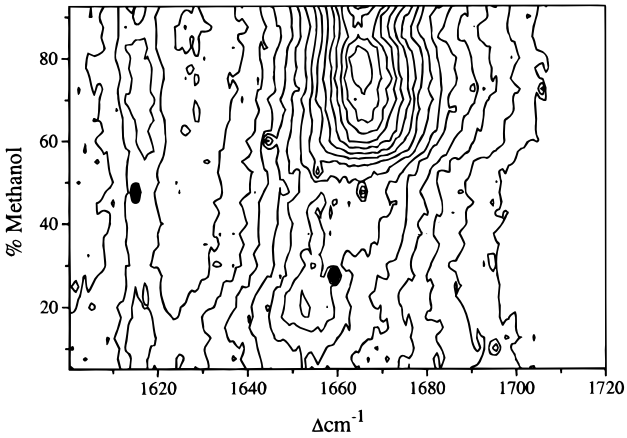

Figure 9. Contour plot of the Raman amide I band of fibroin mapped according to wavenumber and methanol concentration showing the spectral signature for the change in conformation from α-helix (~1650 Δcm^{-1}) to β-sheet (~1670 Δcm^{-1}) with increasing methanol content.

function time while methanol diffused into a 15 wt % solution of fibroin in HFIP. Figure 9 shows the effect of increasing methanol concentration on the position of the amide I band of the fibroin spectra. As the methanol concentration increased during a period of 2.5 h, the position of the amide I band gradually shifted from 1650 to 1670 Δcm^{-1}, which suggests that the dominant fibroin secondary structure changed from α-helix to β-sheet. Multivariate calibration was used to quantify this conformational change (Figure 10).

Fibroin in pure HFIP solution has over 50% helix (combined α-helix and disordered helix). As the methanol concentration increased to 25% by volume, the helical content increased to approximately 70%. At methanol concentrations greater than 30 vol %, the quantity of α-helix decreased and the quantity of β-sheet increased steadily with increasing methanol concentration. When the solution contained approximately 45 vol % methanol, the fibroin exhibited nearly equal quantities of α-helix and β-sheet. At equilibrium (approximately 7% HFIP and 93% methanol by volume) fibroin adopted a 65% β-sheet structure and had precipitated from solution (sample was turbid). These findings are in direct agreement with previous studies, which have shown that polar organic solvents, such as methanol, cause fibroin to adopt a β-sheet structure.[7,13−15]

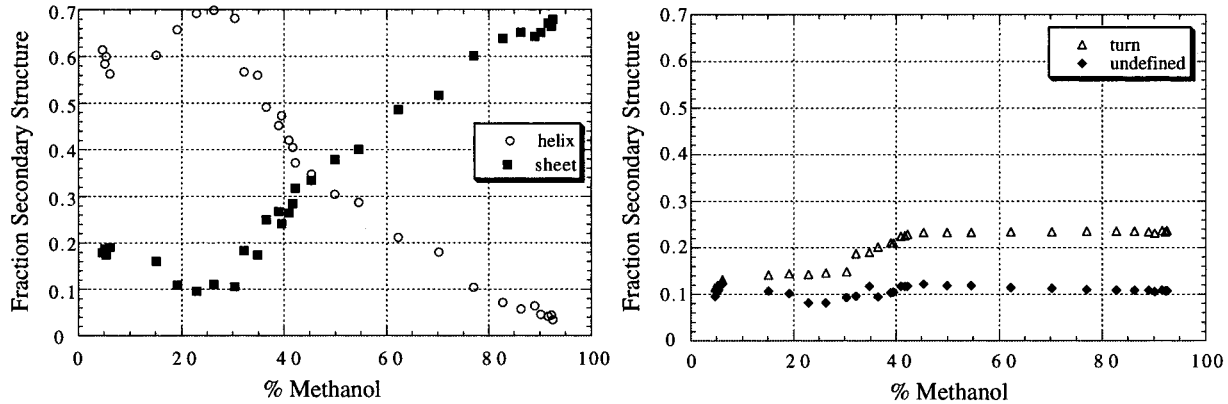

Figure 10. Multivariate statistical analysis of Raman spectra taken as methanol diffused into HFIP solvated fibroin. Plots show the fractions of helix, sheet, turn, and undefined structures (±5%) as a function of methanol concentration. As methanol concentration increases the α-helical structures are converted to β-sheet. The 10% increase in β-turn is consistent with this conformational change.

While the molecular and crystalline structures of these highly drawn SS-fibroin fibers are very similar to those of NS-fibroin fibers, both the Raman spectra and X-ray diffraction patterns show evidence that SS-fibers are more disordered than NS-fibers. X-ray diffraction patterns show that the major equatorial peak width of highly drawn SS-fibers (Figure 6c) is much broader than that of the NS-fibers (Figure 6d), suggesting that the crystals of the SS-fibroin are smaller and/or more disordered than those of NS-fibroin. Likewise, Raman spectra of SS-fibroin fibers show much less detail than the spectra of NS-fibroin fibers. For example, two clearly separable peaks under the amide III band of NS-fibroin (Figure 4a) are broadened in drawn SS-fibroin (Figure 4c) to the point where they are no longer clearly distinguishable. Other processing conditions must be responsible, in part, for the well-ordered structure of NS-fibroin fibers.

Conclusions

B. mori fibroin is an outstanding model protein for understanding how protein-based polymers can be spun into high-performance fibers. The predominantly α-helical structure, which fibroin adopts in HFIP, dramatically changes to an insoluble crystalline β-sheet structure upon synthetic spinning. This conversion to β-sheet structure is caused by the methanol coagulation bath used during wet spinning. The β-sheet crystallites in the undrawn fiber are randomly oriented; however, the elongational flow of the postspinning draw aligns these crystallites and the polypeptide backbone with the fiber axis in addition to converting approximately 5% of the helical structure to β-sheet with a postspinning draw of 3.5. The hierarchical structure observed in naturally-spun fibroin fibers can be best approximated in fibers synthetically spun from HFIP by including a postspinning draw of at least 2.5. Continuing this project to map fibroin conformation onto the synthetic spinning of *B. mori* fibroin fibers will aid in the practical application of recombinantly produced novel biopolymers as useful materials as well as yield insight into the natural *B. mori* fiber spinning process.

Acknowledgment. Funding for this project was provided by the National Institutes of Health Biotechnology Training Grant T32GM08437, National Science Foundation Grant BCS-9202007, the American Association of University Women Educational Foundation Selected Professions Fellowship, and the Whitaker Foundation. The computer code for the multivariate calibration of Raman spectra was provided by Professor Robert W. Williams of the Uniformed Services University of the Health Sciences. Facilities and expertise for X-ray fiber diffraction were provided by Stewart Turley in the Department of Biostructure at the University of Washington. Software for X-ray fiber diffraction analysis was written by Paul Carlson in our laboratory. Silk yarn was obtained through the gracious donation of the Chul Thai Silk Co., Ltd. (Petchboon, Thailand). Finally, we thank Simina Petrovan all her work in maintaining our laboratory and for raising and dissecting silkworms used in these experiments.

References and Notes

(1) Gosline, J. M.; DeMont, M. E.; Denny, M. W. *Endeavour* **1986**, *10*, 37−43.
(2) Xu, M.; Lewis, R. V. *Proc. Natl. Acad. Sci.* **1990**, *87*, 7120−7124.
(3) Lewis, R. V. *Acc. Chem. Res.* **1992**, *25*, 392−398.
(4) Kaplan, D. L.; Fossey, S.; Mello, C. M.; Arcidiacono, S.; Senecal, K.; Muller, W.; Stockwell, S.; Bekwitt, R.; Viney, C.; Kerkam, K. *MRS Bull.* **1992**, October, 41−47.
(5) Hinman, M. B.; Lewis, R. V. *J. Biol. Chem.* **1992**, *267*, 19320−19324.
(6) Asakura, T.; Kuzuhara, A.; Tabeta, R.; Saito, H. *Macromolecules* **1985**, *18*, 1841−1845.
(7) Iizuka, E.; Yang, J. T. *Biochemistry* **1968**, *7*, 2218−2228.
(8) Asakura, T.; Suzuki, H.; Watanabe, Y. *Macromolecules* **1983**, *16*, 1024.
(9) Asakura, T.; Kashiba, H.; Yoshimizu, H. *Macromolecules* **1988**, *21*, 644.
(10) Marsh, R. E.; Corey, R. B.; Pauling, L. *Biochim. Biophys. Acta* **1955**, *16*, 1−34.
(11) Gillespie, D. B.; Viney, C.; Yager, P. In *Silk Polymers: Materials Science and Biotechnology*; Kaplan, D., Adams, W. W., Farmer, B., Viney, C., Eds.; American Chemical Society: Washington, DC, 1994; pp 155−167.
(12) Asakura, T.; Yeo, J.-H.; Demura, M.; Itoh, T.; Fujito, T.; Imanari, M.; Nicholson, L. K.; Cross, T. A. *Macromolecules* **1993**, *26*, 6660−6663.
(13) Iizuka, E.; Yang, J. T. *Proceedings of the National Academy of Science* **1966**, *55*, 1175−1182.
(14) Magoshi, J.; Mizuide, M.; Magoshi, Y.; Takahashi, K.; Kubo, M.; Nakamura, S. *J. Polym. Sci.: Polym. Phys. Ed.* **1979**, *17*, 515−520.
(15) Venyaminov, S. Y.; Kalnin, N. N. *Biopolymers* **1990**, *30*, 1259−1271.
(16) Iizuka, E. *J. Appl. Polym. Sci., Appl. Polym. Symp.* **1985**, *41*, 173−185.
(17) Iizuka, E. *Biorheology* **1966**, *3*, 141−152.
(18) Yamaura, K.; Okumura, Y.; Matsuzawa, S. *J. Macromol. Sci.-Phys. B* **1982**, *21*, 49−69.
(19) Yamaura, K.; Okumura, Y.; Oazki, A.; Matsuzawa, S. *J. Appl. Polym. Sci.: Appl. Polym. Symp.* **1985**, *41*, 205−220.
(20) Magoshi, J.; Magoshi, Y.; Nakamura, S. *J. Appl. Polym. Sci., Appl. Polym. Symp.* **1985**, *41*, 187−204.
(21) Asakura, T.; Demura, M.; Date, T.; Miyashita, N.; Ogawa, K.; Williamson, M. P. *Biopolymers* **1997**, *41*, 193−203.
(22) Anderson, J. P.; Cappello, J.; Martin, D. *Biopolymers* **1994**, *34*, 1049−1057.
(23) Simmons, A. H.; Michal, C. A.; Jelinski, L. W. *Science* **1996**, *271*, 84−87.
(24) Kummerlen, J.; Van Beek, J. D.; Vollrath, F.; Meier, B. H. *Macromolecules* **1996**, *29*, 2920−2928.
(25) Anderson, J. P.; Stephen-Hassard, M.; Martin, D. C. In *Silk Polymers: Materials Science and Biotechnology*; Kaplan, D., Adams, W. W., Farmer, B., Viney, C., Eds.; American Chemical Society: Washington, DC, 1994; pp 137−154.
(26) Viney, C.; Huber, A. E.; Dunaway, D. L.; Kerkam, K.; Case, S. T. In *Silk Polymers: Materials Science and Biotechnology*; Kaplan, D., Adams, W. W., Farmer, B., Viney, C., Eds.; American Chemical Society: Washington, DC, 1994; pp 120−136.
(27) Lock, R. L. In *WO93/15244*; E. I. Du Pont De Nemours and Company: Wilmington, DE, 1993.
(28) Suzuki, Y.; Brown, D. D. *J. Mol. Biol.* **1972**, *63*, 409−429.
(29) Gillespie, D. B.; Thiel, B. L.; Trabbic, K. A.; Viney, C.; Yager, P. *Macromolecules* **1994**, *27*, 6177−6182.
(30) Williams, R. W. *J. Mol. Biol.* **1983**, *166*, 581−603.
(31) Alexander, L. E. ; Robert E. Krieger Publishing Company: Malabar, FL, 1969; pp 262−268.
(32) Williams, R. W. *Methods Enzymol.* **1986**, *130*, 311−353.
(33) Canetti, M.; Seves, A.; Secundo, G.; Vecchio, F. *Biopolymers* **1989**, *28*, 1613−1624.
(34) Parrish, J. R. J.; Blout, E. R. *Biopolymers* **1972**, *11*, 1001−1020.
(35) Lucas, F.; Shaw, J. T. B.; Smith, S. G. *Biochem. J.* **1957**, *66*, 468.

MA9708860